Transactions on Computer Science and Intelligent Systems Research
ISSN: 2960-1800, eISSN: 2960-2238 | Volume 11
TPCEE 2025

Investigation into the Chaoticity Systems of Galaxy Triplets Based on the N-Body Numerical Simulation

Yinqi Wu

Chengdu No.7 High School International Department, Chengdu, Sichuan, 610000, China

qwyndrzo@krae.edu.kg

Abstract. With more attention being put on the dynamic evolution of celestial bodies, the system of galaxy triplets has been considered as an important and helpful dynamic system to understand the gravitational interaction between stars and clusters in the universe. However, the analysis of the chaoticity of the system of galaxy triplets was still not emphasized as much as the system of three point masses. By setting the same initial conditions of L4 on the system of extended masses and the system of point masses, and using chaos indicators, including Mean Exponential Growth of Nearby Orbits and Maximum Lyapunov Exponent, the chaoticity of each system is quantified and compared. The paper found that many orbits of extended masses are likely to be more stable than orbits of point masses. A possible explanation for this result is that the dynamic friction between extended masses dissipates the system's energy, contributing to fewer unbounded orbits. Hence, more orbits are likely to be stable and bounded.

Keywords: Galaxy triplets; chaoticity; initial conditions; N-body simulation.

1. Introduction

Systems of galaxy triplets play an important role in the evolution of the universe. They are galaxy groups with the least number of galaxies and are natural laboratories that can provide insight into the formation of larger groups and perhaps even clusters [1]. Unlike traditional three-body systems, extended mass models are used for the simulation of galaxy triplets instead of mass points. These models provide a more realistic dynamic simulation of celestial bodies. However, compared to the traditional three-body problem, galaxy triplets, or the three-galaxy problem, have not been emphasized or analyzed as much.

In terms of the observation of galaxy triplets, Karachentseva et al. were the first to compile a systematic catalogue of triplets and to study some of their observational properties [2]. Years later, several optical methods were invented to identify the state of interaction between galaxies, including the synergy of R-band (optical) and K-band (near-infrared) imaging, Visual Morphological Classification, and multi-wavelength imaging (BVRI, SDSS RGB, and 2MASS NIR). These methods investigated the morphologies, star formation region properties, and colour distribution of galaxy interactions [3-5]. These studies provided a sound base and abundant data for further simulation and investigation of the galaxy triplets. In the realm of numerical simulations, Aceves first used a self-gravitating galaxy model (Plummer model) to simulate the dynamical evolution of galaxy triplets, providing a crucial benchmark of the three-galaxy problem [6]. More recently, by combining Illustris simulations with post-processed triple dynamics models, Satheesh et al. quantified a 4% increase in the total MBH merger fraction due to strong triple interactions. It was the first to qualify the impact of strong triple dynamics on the merger of MBH [7].

The main goal of this paper is to compare the chaoticity of the systems of galaxy triplets and three-point masses, and the sensitivity of the system of galaxy triplets to the initial conditions. This work is divided as follows. In Section 2, solutions and models are described, and the initial condition is set. In Section 3, the simulation of the evolution and the analysis of the results of the simulations are done. In Section 4, the analysis results are discussed.

2. Initial Conditions and Methods

2.1. Models and Initial Conditions

In the simulations of galaxy triplets in this paper, the Plummer model and the King model are used as extended mass models. The Plummer model was originally introduced by H.C. Plummer in 1911 and is widely utilised in the simulation of celestial bodies and extended masses due to its simplicity. The Plummer model assumes a static equilibrium configuration with a finite central density and a steep decline in density at large radii, ensuring a finite total mass. Its density distribution function is expressed by:

$$\rho(r) = \frac{3M}{4\pi a^3}(1 + \frac{r^2}{a^2})^{-\frac{5}{2}} \tag{1}$$

Where M is the total mass, a is the scale length, and r is the radial distance. Its gravitational potential is described by

$$\Phi(r) = -\frac{GM}{\sqrt{r^2+a^2}} \tag{2}$$

The King model was first proposed by Ivan R. King in 1966. It is a widely used empirical model for describing the spatial structure of self-gravitating stellar systems. The model assumes a lowered isothermal distribution function and a truncated density profile, characterised by a finite tidal radius. Compared to the Plummer model, the King model incorporates a tidal cutoff that better reflects the finite extent of real stellar systems embedded in external gravitational fields. Its distribution function is in the form of a lowered isothermal distribution:

$$f(E) = \begin{cases} A(e^{\frac{-E}{\sigma^2}} - 1), E < 0 \\ 0, \qquad E \geq 0 \end{cases} \tag{3}$$

Where, $E = \Psi(r) - \frac{1}{2}v^2$ is the relative energy of a star at position r and speed v; $\Psi(\mathrm{R}) = \Phi_t - \Phi(r)$ is the relative potential, defined so that Ψ=0 at the tidal radius; $\Phi(r)$ is the gravitational potential at radius r ; Φ_t is the tidal potential ; σ is the velocity dispersion; A is a normalisation constant.

Its density profile is described as

$$\rho(r) = 4\pi \int_0^{\sqrt{2\Psi(r)}} f(\Psi(r) - \frac{1}{2}v^2)v^2\, dv \tag{4}$$

This integral is usually evaluated numerically or tabulated as a function of the dimensionless potential $W = \frac{\Psi}{\sigma^2}$.

As for the gravitational potential of the King model, it is solved from the Poisson equation:

$$\frac{1}{r^2}\frac{d\left(r^2\frac{d\Psi}{dr}\right)}{dr} = -4\pi G\rho(r) \tag{5}$$

This equation is typically solved numerically with boundary conditions.

To compare with the traditional three-body systems, classic Lagrange solutions, especially L4 and L5, are chosen as the initial conditions for the simulation. In L4, the three mass points are set at the vertices of an equilateral triangle. The angular velocity of the three mass points is given by

$$\omega = \sqrt{\frac{G(m_1+m_2+m_3)}{a^3}} \quad (6)$$

Where m1, m2, and m3 are the masses of the three mass points respectively, and a is the edge length of the equilateral triangle. In this simulation, N-body units were used instead of traditional units for simplicity. Every cluster was set to have 1000 stars initially, and the mass of each cluster was set to be 1. The gravitational constant was set as 1.

2.2. Analytic Methods and Simulations

In this paper, NEMO (a stellar dynamics toolbox) was used for simulations. It is a collection of programs running under a standard UNIX shell, capable of executing various stellar dynamical codes and related utilities (initialisation, analysis, gridding, orbits) [8]. Several N-body models and integrators are pre-configured in it. By setting different initial conditions, 26 sets of simulations were conducted to investigate the differences between mass points and extended mass in the three-body system, as well as the impact of scale length, central concentration parameter, gravitational softening length, and the initial distance between clusters. For numerical integration, gyrfalcON, which stands for galaxy simulator using Walter Dehnen's force algorithm of complexity O(N), was used. The code benefits from an improved and simple multipole acceptance criterion that reduces force error and computational effort. For $N>\sim10^4$, the computational costs are empirically observed to rise sublinearly with N [9].

Every orbit evolved for 100 steps. To compare the chaoticity of the three-body systems, the Maximum Lyapunov Exponents (MLEs) of every orbit were calculated. Based on the MLEs, K-means clustering was used to separate the orbits into 3 groups. The Mean Exponential Growth factor of Nearby Orbits (MEGNO) of representative orbits in each group was also calculated to analyze the variation of chaoticity of the systems. To analyse the sensitivity of each system to the initial conditions, Random Forest (RF) was used to calculate the feature importance of each initial condition.

3. Results

Before the simulation, every orbit was divided into 2 groups: the Plummer group and the King group. In the Plummer group, the extended mass model used in the simulation was the Plummer model; in the King group, the extended mass model was the King model. For every initial condition, 5 different values were set to simulate different orbits. The list of the initial conditions of different orbits is shown in Table 1.

As for the initial conditions of the three-body system of point masses, the initial side length was set to be 2, which was the same as the benchmark orbits of each group.

Before the simulation, the value of the Virial ratio of each system was calculated to determine the unbound orbits. The values of the Virial ratio of the orbits P9, K8, and K9 were much greater than 1, which indicated that these orbits were unbound. Thus, further simulation of these orbits was not done.

Table 1. The list of initial conditions. The serial number indicates the group of orbits. P means the orbit belonged to the Plummer group. K means the orbit belonged to the King group. The orbits P1 and K1 were considered as the benchmark orbits of each group

Serial number	Side length	Gravity softening length	Scale length	Dimensionless central potential
P1	2.00	0.050	1.00	-
P2	4.00	0.050	1.00	-
P3	6.00	0.050	1.00	-
P4	8.00	0.050	1.00	-
P5	10.0	0.050	1.00	-
P6	2.00	0.050	0.50	-
P7	2.00	0.050	0.75	-
P8	2.00	0.050	1.25	-
P9	2.00	0.050	0.25	-
P10	2.00	0.100	1.00	-
P11	2.00	0.075	1.00	-
P12	2.00	0.125	1.00	-
P13	2.00	0.025	1.00	-
K1	2.00	0.050	-	6.00
K2	4.00	0.050	-	6.00
K3	6.00	0.050	-	6.00
K4	8.00	0.050	-	6.00
K5	10.0	0.050	-	6.00
K6	2.00	0.050	-	2.00
K7	2.00	0.050	-	4.00
K8	2.00	0.050	-	8.00
K9	2.00	0.050	-	10.0
K10	2.00	0.100	-	6.00
K11	2.00	0.075	-	6.00
K12	2.00	0.125	-	6.00
K13	2.00	0.025	-	6.00

3.1. The Results of the Simulation

3.1.1. The Plummer group.

Table 2. The MLE values of each orbit in the Plummer group and the clustering result

Serial number	MLE	Clustering group
P1	0.06983	Middle chaotic
P2	0.07815	High chaotic
P3	0.05862	Middle chaotic
P4	0.06228	Middle chaotic
P5	0.04215	Low chaotic
P6	0.06749	Middle chaotic
P7	0.07359	High chaotic
P8	0.07724	High chaotic
P10	0.07543	High chaotic
P11	0.06043	Middle chaotic
P12	0.06503	Middle chaotic
P13	0.08154	Middle chaotic

The MLE values of every orbit in the Plummer group are listed in Table 2. Based on the MLE values, K-means clustering was used to divide the orbits into three groups. The result of the clustering is also shown in Table 2.

For comparison, the MLE value of the point-mass orbit was also calculated, which was 0.34406. The orbits P3, P5 and P7 were selected to represent each clustering group. Fig. 1 presents the variation of their MEGNO values. For the comparison, the variation of MEGNO values is also shown in Fig. 1.

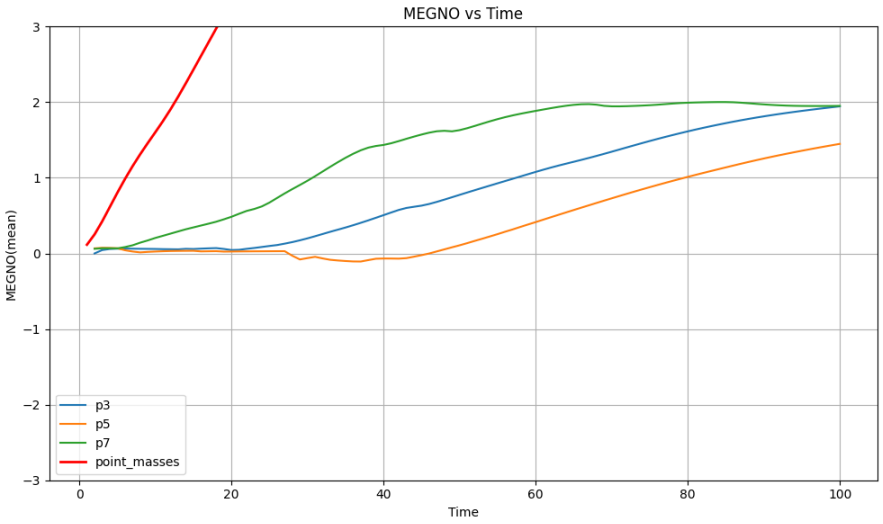

Figure 1. The MEGNO values of the orbits P3, P5, and P7 and the point-mass orbit (Photo/Picture credit: Original)

The x-axis of Fig. 1 is the time of the evolution, and the y-axis is the mean MEGNO values. The results of MEGNO values and MLE values were in good agreement with each other. The MLE value of the point-mass orbit was higher than 4 times the highest MLE value in the Plummer models. As for the MEGNO values, the increasing rate of the MEGNO values of the point-mass orbit was much higher than the others, which can be seen in Fig. 1. In terms of the variation of the MEGNO values of the extended-mass orbits, the increasing rates also agreed well with the MLE values and the clustering result. However, the MEGNO values of these orbits showed a trend of convergence to 2 at the end of the simulation, which indicated that all these orbits were relatively weakly chaotic.

3.1.2. The king group.

The MLE values of the orbits in the King group, as well as the clustering result based on the MLE values, are given in Table 3.

Table 3. The MLE values and the clustering results of the orbits in the King group

Serial number	MLE	Clustering group
K1	0.06226	Middle chaotic
K2	0.06911	Middle chaotic
K3	0.04740	Low chaotic
K4	0.05475	Low chaotic
K5	0.04366	Low chaotic
K6	0.07518	High chaotic
K7	0.08122	High chaotic
K10	0.06000	Middle chaotic
K11	0.06832	Middle chaotic
K12	0.06592	Middle chaotic
K13	0.07768	High chaotic

The orbits K5, K7 and K11 were selected to represent each group. The variation of the MEGNO values of these orbits and the point-mass orbit versus time is illustrated in Fig. 2.

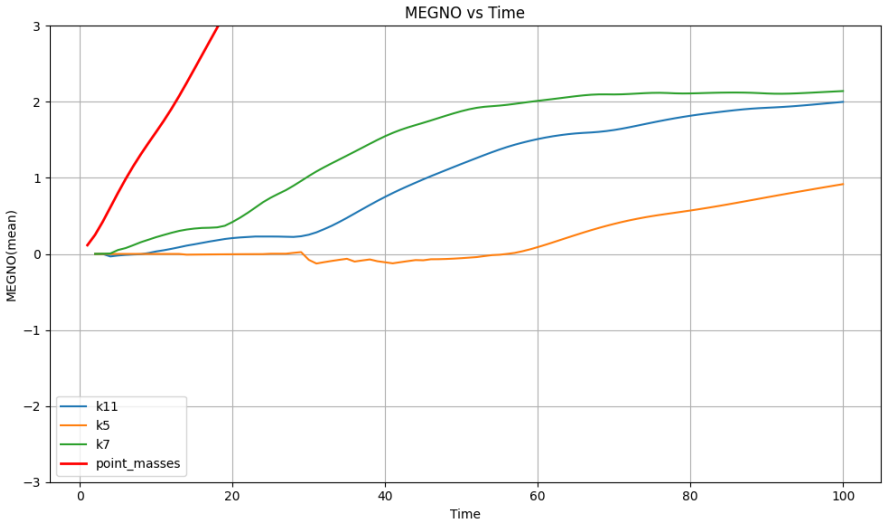

Figure 2. The variation of the MEGNO values of the orbits K5, K7, and K11 and the point-mass orbits (Photo/Picture credit: Original)

The x-axis of Fig. 2 is the time of the evolution, and the y-axis is the mean MEGNO values. The MEGNO values of the orbit K5 were the most stable, fluctuating around 0 in the first 60 steps and increasing slowly after 60 steps. Despite the different increasing rates, the variation trend of the MEGNO values of the orbits K7 and K11 was similar: increasing quickly at first, then converging to 2 at the end of the simulation. The increasing rate of the point-mass orbit was still high compared with the orbits in the King group, which was in good agreement with its high MLE value.

3.2. The Results of Data Analysis

3.2.1. The comparison of the chaoticity of three-body systems.

The initial side length of the system of point masses was changed for the comparison. The initial side length and MLE values of different point-mass orbits are listed in Table 4.

Table 4. The initial side length and the MLE values of the point-mass orbits

Serial number	Initial side length	MLE
M1	2.00	0.34406
M2	0.25	0.17108
M3	0.50	0.12985
M4	0.75	0.10625
M5	1.00	0.10278
M6	1.25	0.30361

Fig. 3 presents the distribution of the MLE values obtained for the orbits in the Plummer, King, and the point-mass groups, shown as a boxplot.

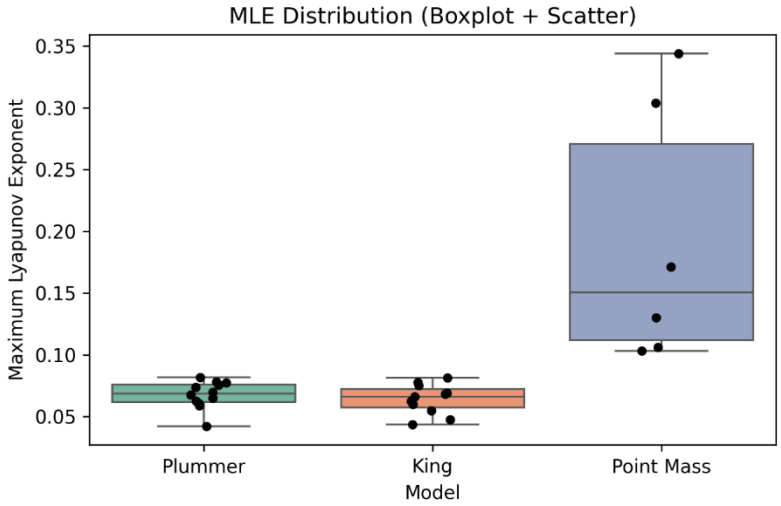

Figure 3. Boxplot of the MLE values for the orbits in Plummer, King and point-mass groups (Photo/Picture credit: Original)

The point-mass model exhibited a higher median value, approximately 0.15. The median values of the Plummer and the King models were almost the same, maintaining around 0.07, which was half the value of the point-mass model. The interquartile range of the MLE values of point-mass orbits was also substantially wider than that of extended-mass orbits.

The distribution of MLE values is also displayed as a KDE plot in Fig. 4.

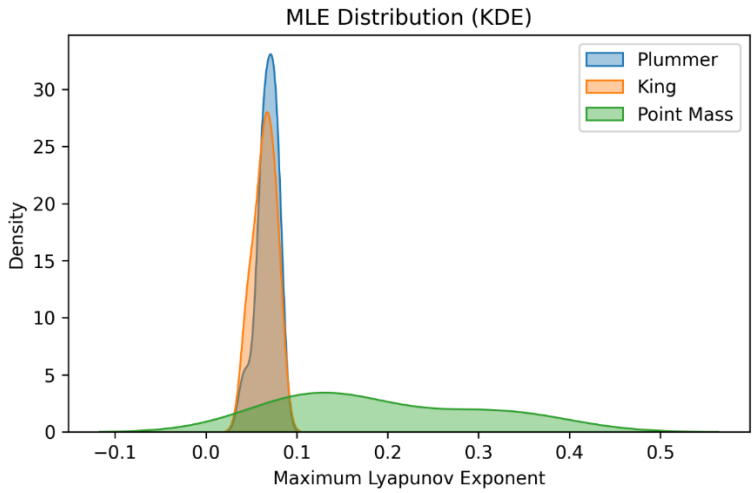

Figure 4. KDE plot of the MLE values of the orbits in the Plummer, King, and point-mass groups (Photo/Picture credit: Original)

Fig. 4 shows that the MLE values of the orbits in the Plummer and the King group had similar, sharply peaked distributions centred near 0.07-0.08, while that of the point-mass orbits exhibits a broader distribution with a secondary tail extending beyond 0.3.

3.2.2. The Sensitivity Analysis of the Initial Conditions.

Fig. 5 illustrates the results of the sensitivity analysis of the initial conditions in both the three-body system of the Plummer models and the system of the King models.

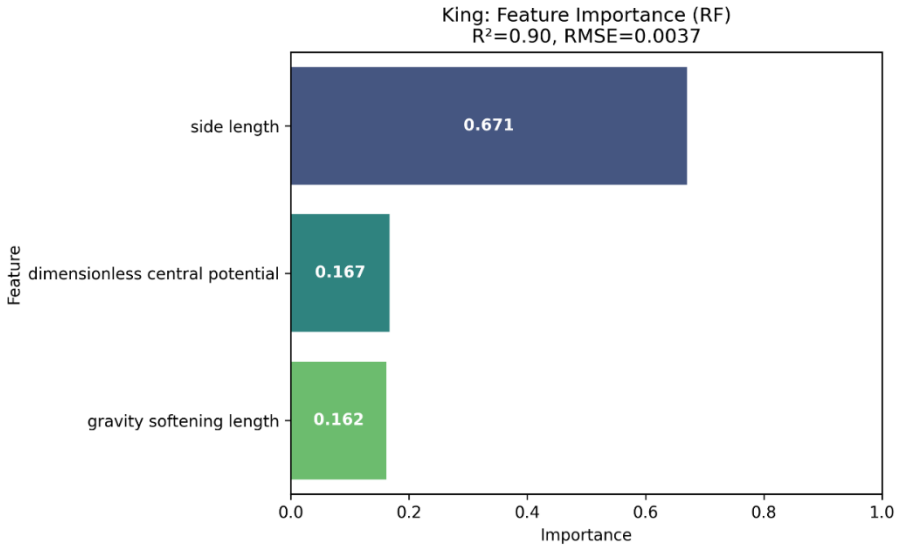

Figure 5. The feature importance of the initial conditions in the King group (Photo/Picture credit: Original)

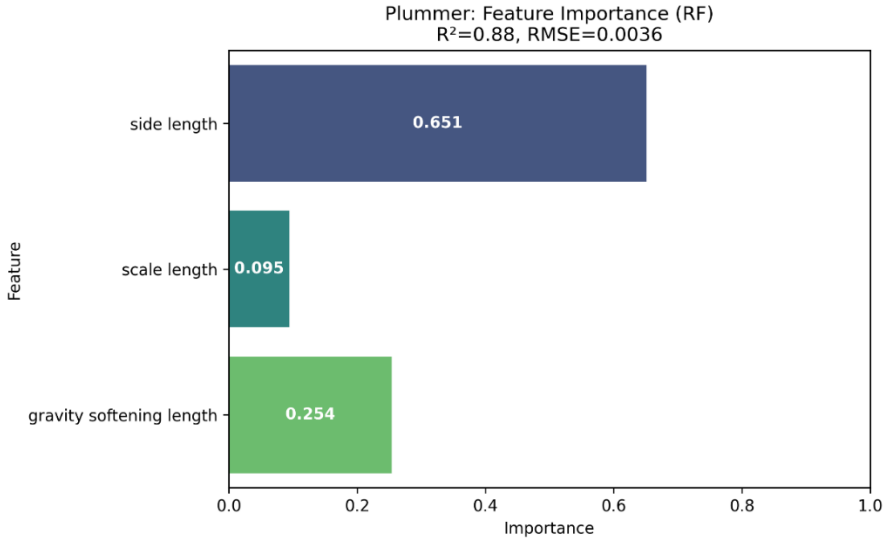

Figure 6. The feature importance of the initial conditions in the Plummer group (Photo/Picture credit: Original)

The x-axis of Fig. 5 and Fig. 6 is the importance of the initial conditions, spanning from 0.0 to 1.0, and the y-axis is the initial conditions. According to Fig. 5 and Fig. 6, both the three-body system of the Plummer models and the system of the King models are the most sensitive to the initial side length. In the Plummer group, the importance of the initial side length was 0.651, and in the King group, it was 0.671. However, the system of the Plummer models was more sensitive to the gravity softening length. In the Plummer group, the importance of the gravity softening length was approximately 3 times that of the scale length, while in the King group, the importance of the dimensionless central potential and the gravity softening length was almost the same.

4. Conclusion

This paper talks about the comparison of chaoticity between the three-body system of point masses and the system of galaxy triplets. The mean MLE of three-body systems of point masses was about 2 times that of the system of galaxy triplets, which revealed that the system of galaxy triplets is more likely to form weakly chaotic orbits. This result echoes the findings of Amira A. Tawfeek et al. In addition, the wider interquartile range of the MLEs of point-mass orbits indicates that the sensitivity of the extended-mass systems to the initial conditions is much lower than that of point-mass systems.

A possible reason for these results is that the dynamic friction between extended masses dissipates the energy of the system, contributing to fewer unbound orbits. The paper also found that, similar to the classic three-body system of point masses, the initial conditions have an impact on the chaoticity of the system, which echoes the findings of Aceves. Additionally, the sensitivity of different systems to different initial conditions was also quantified. In the three-body systems of the Plummer models and the King models, the initial side length of the equilateral triangle influenced the MLE of the orbit the most. This may be because, as the initial side length decreases, the clusters merge more quickly, which contributes to a more unpredictable behaviour of the centre of mass of clusters due to interaction between stars.

The findings of this paper provide a reference for the research on the dynamic evolution of extended mass systems, especially for the setting of initial conditions of extended masses. However, the research in this paper still has considerable potential for improvement. First, due to the limitations of time and computing power, only 23 N-body simulations were taken for the analysis. More N-body simulations should be taken for a better qualification of the sensitivity to initial conditions and the comparison between extended-mass orbits and point-mass orbits. Second, more different initial conditions and different N-body models could be attempted in future research.

References

[1] Hernández-Toledo H M, Cano-Díaz M, Valenzuela O, Puerari I. The bulgeless Seyfert/LINER galaxy NGC 3367: disk, bar, lopsidedness, and environment. Astronomical Journal, 2011, 142 (6): 182.

[2] Karachentseva V E, Karachentsev I D. Isolated triplet of galaxies. Astrofizicheskie Issledovaniia Izvestiya Spetsial'noj Astrofizicheskoj Observatorii, 1979, 11: 3–17.

[3] Veilleux S, Kim D C, Sanders D B. Optical and near-infrared imaging of the IRAS 1 Jy sample of ultraluminous infrared galaxies. II. The analysis. Astrophysical Journal Supplement Series, 2002, 143 (2): 315–370.

[4] Hernández-Toledo H M, Cano-Díaz M, Valenzuela O, Puerari I. The bulgeless Seyfert/LINER galaxy NGC 3367: disk, bar, lopsidedness, and environment. Astronomical Journal, 2011, 142 (6): 182.

[5] Kilerci Eser E, Goto T, Doi Y. Ultraluminous infrared galaxies in the AKARI all-sky survey. Astrophysical Journal, 2014, 797 (1): 54.

[6] Aceves H. Dynamical evolution of triplets of galaxies. Monthly Notices of the Royal Astronomical Society, 2001, 326 (4): 1412–1424.

[7] Souvaitzis L, Rantala A, Naab T. The role of massive black holes in merging star clusters: dynamical evolution, stellar and compact object ejections, and gravitational waves. Monthly Notices of the Royal Astronomical Society, 2025, 539 (1): 45–64.

[8] Teuben P J. NEMO users and programmers guide (Version 4.0-MD). Astronomy Department, University of Maryland, 2018.

[9] Dehnen W. A very fast and momentum-conserving tree code. Astrophysical Journal, 2000, 536 (1): L39–L42.